Comparison of $\nu_{\mu} \leftrightarrow \nu_{\tau}$ and $\nu_{\mu} \leftrightarrow \nu_{s}$ oscillations as solutions of the atmospheric neutrino problem

Paolo Lipari and Maurizio Lusignoli Dipartimento di Fisica, Università di Roma "la Sapienza", and I.N.F.N., Sezione di Roma, P. A. Moro 2, I-00185 Roma, Italy

Abstract

The simplest explanation for the atmospheric neutrino anomaly is the transition of muon neutrinos and antineutrinos into states of different flavor. Data from the reactor experiment Chooz, and the measurement of the energy and angle distribution of electron–like events in Super–Kamiokande put strong constraints on ν_{μ} – ν_{e} mixing, but the transitions $\nu_{\mu} \rightarrow \nu_{\tau}$ and $\nu_{\mu} \rightarrow \nu_{s}$ are viable possibilites. If the muon neutrinos are mixed with a singlet sterile state, the energy and zenith angle dependence of the oscillation probability is modified by matter effects, that are important for $E_{\nu}/|\Delta m^{2}| \gtrsim 10^{3} \text{ GeV/eV}^{2}$. We confront the theoretical predictions with existing data on contained events and neutrino–induced upward going muons.

1 Introduction

Recent results on atmospheric neutrinos [1, 2] show a deficit in the number of ν_{μ} -induced events that can be interpreted as a consequence of neutrino oscillations. Additional signals of ν -oscillations come from solar neutrinos [3] and from the LSND experiment [4]. These results, if all interpreted in terms of oscillations, require three independent values of the parameter Δm^2 , seem to imply the existence of a least four neutrino mass eigenstates [5] and therefore, given the limits on the number of flavors of standard neutrinos [10], the existence of at least one sterile state.

The energy and zenith angle distributions of the electron–like events detected by Super–Kamiokande [2] are in agreement with the Montecarlo prediction without oscillations; at the same time, the results of the Chooz experiment [9] put stringent limits on ν_{μ} – ν_{e} mixing in the region of Δm^{2} of interest, therefore the hypothesis of $\nu_{\mu} \leftrightarrow \nu_{e}$ oscillations as explanation of the atmospheric neutrino data is disfavored (see [11] and [12] for

a more quantitative discussion). The atmospheric neutrino data can be explained by the existence of $\nu_{\mu} \leftrightarrow \nu_{\tau}$ or $\nu_{\mu} \leftrightarrow \nu_{s}$ oscillations, where ν_{s} is a sterile neutrino. The possibility that the atmospheric neutrino anomaly is due to ν_{μ} – ν_{s} mixing has been previously discussed in [13], and more recenty in [14, 15, 16, 17].

Bounds on the existence of sterile states with large mixing to the standard neutrinos have been obtained from cosmological considerations [18]. For large enough values of the mixing angle and Δm^2 , the oscillations of standard into sterile neutrinos can bring the sterile states in (or close to) thermal equilibrium with matter before the nucleosynthesis epoch. The increase in the energy density results in the overproduction of primordial helium, spoiling the success of Big Bang Nucleosynthesis. Schramm and Turner [19], have estimated the upper limit (at 95 % C.L.) on the number of light degrees of freedom at nucleosynthesis as $N_{\nu} \leq 3.6$. This bound, according to the analyses in [18], is incompatible with the explanation of the atmospheric neutrino problem as due to the mixing betwen muon and sterile neutrinos, because the allowed region in the oscillation parameter space would result in $N_{\nu} \simeq 4$. However recent work [20] has shown that this cosmological bound can be evaded, considering the suppression of oscillations due to the possible presence of a lepton asymmetry in the early universe that can be generated by the oscillations themselves.

It is interesting to investigate if the data on atmospheric neutrinos already existing or to be collected in the near future can discriminate between these two different hypotheses for oscillations. The energies of atmospheric neutrinos are such that only a very small fraction is above the threshold for τ -lepton charged current (CC) production, on the other hand the neutral current (NC) cross sections of ν_{τ} and ν_{μ} are identical. Sterile neutrinos instead, by definition, do not interact even by neutral currents. In principle the presence of a flux of tau neutrinos can therefore be identified as an excess of NC over CC events. The measurement is possible in large mass detectors like Super-Kamiokande (SK). The most promising method, as recently discussed by Smirnov and Vissani [15], is the study of the reaction $\nu_x N \to \nu_x N \pi^{\circ}$ where a single π° is produced, and detected after its decay $\pi^{\circ} \to \gamma \gamma$. The absolute value of the cross section for this process is not known with great accuracy, because it has only been measured with large errors [21] and it is difficult to compute theoretically [22]. Part of this uncertainty should cancel [15] when comparing with the rate of single pion events produced in charged-current interactions. Experimentally one will need to know with sufficient accuracy the acceptance and efficiency for the detection of events with at least two 'tracks' in the final state.

Another handle to distinguish the ν_{μ} – ν_{τ} and ν_{μ} – ν_{s} mixing is given by the fact that the energy and zenith angle dependence of the oscillation probabilities are different in the two cases because of the presence of matter effects [23]. In this work we discuss in detail this possibility, examining the effects that could be observed both in the events induced by neutrino interactions in the detector and in the upward going muons, generated by neutrino interactions in the rock beneath the detector. As we will show, the most promising tool to disentangle matter effects should be provided by the study of upward going muons, notwithstanding the present confusing experimental situation.

2 Matter effects and oscillation probabilities

2.1 Oscillation parameters in matter

The $\nu_{\alpha} \to \nu_{\beta}$ oscillation probability in vacuum, in the simple case of two flavor mixing, is given by the standard formula:

$$P_{\nu_{\alpha} \to \nu_{\beta}} = \sin^2 2\theta \sin^2 \left(\frac{\Delta m^2 L}{4E_{\nu}}\right) \equiv \sin^2 2\theta \sin^2 \left(\pi \frac{L}{\ell}\right) \tag{1}$$

where θ , defined in the interval $[0, \pi/4]$, is the mixing angle that relates the flavor and mass eigenstates ($|\nu_{\alpha}\rangle = \cos\theta |\nu_{1}\rangle + \sin\theta |\nu_{2}\rangle$, $|\nu_{\beta}\rangle = -\sin\theta |\nu_{1}\rangle + \cos\theta |\nu_{2}\rangle$) and $\Delta m^{2} = m_{2}^{2} - m_{1}^{2}$, with m_{1} and m_{2} the mass eigenvalues.

In the presence of matter with constant density the mixing angle θ and the oscillation length ℓ must be replaced by θ_m and ℓ_m , defined as follows:

$$\sin^2 2\,\theta_m = \frac{\sin^2 2\,\theta}{\left[\zeta - \cos 2\,\theta\right]^2 + \sin^2 2\,\theta},\tag{2}$$

$$\ell_m = \frac{\ell}{\{ [\zeta - \cos 2\theta]^2 + \sin^2 2\theta \}^{1/2}}.$$
 (3)

where

$$\zeta = \frac{2 E_{\nu} V_{\alpha\beta}}{\Lambda m^2} \tag{4}$$

and $V_{\alpha\beta} = V_{\alpha} - V_{\beta}$ is the difference between the effective potentials in matter of neutrinos of flavor α and β [23]. The effective potentials of ν_{μ} ad ν_{τ} in ordinary matter are identical, and matter effects vanish in the case of ν_{μ} – ν_{τ} mixing. In the case of ν_{μ} – ν_{s} mixing the difference in the effective potential is

$$V_{\mu s} = \mp \sqrt{2} G_F \frac{N_n}{2} = \mp 1.9 \cdot 10^{-4} \frac{\text{eV}^2}{\text{GeV}} \left(\frac{\rho}{\rho_o}\right) \left(1 - \frac{Z}{A}\right),$$
 (5)

where the minus (plus) sign is for neutrinos (antineutrinos), G_F is the Fermi constant, N_n the neutron number density, ρ the mass density ($\rho_o = 5$ g cm⁻³ is a reference value) and (1 - Z/A) the neutron fraction. For comparison we note that the effective potential in the case of $\nu_e - \nu_\mu$ mixing is $V_{e\mu} = \pm \sqrt{2}G_F N_e$ where N_e is the electron density; in the earth $N_e \simeq N_n$ and $V_{e\mu} \simeq -2 V_{\mu s}$.

The meaning of equations (2) and (3) is illustrated in figs. 1 and 2, respectively. In these figures we have plotted the oscillation parameters in matter for a fixed value of the density $\rho = \rho_o$ and for values of Δm^2 and $\sin^2 2\theta$ relevant for atmospheric neutrinos. The matter effects are controlled by the ratio ζ defined in eq. (4). For $|\zeta| \ll 1$ (small neutrino energies) the matter effects are negligible, and the oscillations proceed as in vacuum. For $|\zeta| \gg 1$ (large neutrino energies) the matter effects are dominant and the oscillations are strongly supressed: the effective mixing $\sin^2 2\theta_m$ decreases like ζ^{-2} and the oscillation length levels off to a value $\ell_m^\infty = 2\pi/|V_{\mu s}| \simeq 1.3 (\rho_o/\rho) 10^4$ km, independent from E_ν

and Δm^2 , and remarkably close to the earth's diameter. In the region $|\zeta| \sim 1$, that corresponds to a neutrino energy

$$E_{\nu} \sim \frac{|\Delta m^2|}{\sqrt{2}G_F N_n} = 5.2 \text{ GeV} \left(\frac{|\Delta m^2|}{10^{-3} \text{ eV}^2}\right) \left(\frac{\rho_{\circ}}{\rho}\right) ,$$
 (6)

one has the most complex behavior. In general, with the exception of the special case of maximal mixing ($\sin^2 2\theta = 1$), neutrinos and antineutrinos have different oscillation parameters in matter, because of the opposite sign of the effective potential. The effective mixing in matter becomes maximal (MSW resonance effect [23]) when the condition $\zeta = \cos 2\theta$ is satisfied. This is possible for antineutrinos (neutrinos) when Δm^2 is positive (negative) and is illustrated by the curves labeled 'c' and 'd'.

Inspection of figs. 1 and 2 allows to understand qualitatively when the matter effects can be important, and the hypotheses of $\nu_{\mu} \leftrightarrow \nu_{\tau}$ and $\nu_{\mu} \leftrightarrow \nu_{s}$ oscillations experimentally distinguishable. Atmospheric neutrinos have been observed in essentially three energy regions: (a) the sub–GeV region: events with charged lepton energy in the range 0.1–0.2 $\leq E_{\ell} \leq 1.33$ GeV, produced by neutrinos with average energy $\langle E_{\nu} \rangle \simeq 0.7$ –0.8 GeV; (b) the multi–GeV region: events with charged lepton energy in the interval $E_{\ell} \geq 1.33$ GeV, produced by neutrinos with $\langle E_{\nu} \rangle \simeq 7$ GeV; (c) upward–going muons, produced by a broad range of neutrino energies with a median energy of order 100 GeV. The analyses of the sub–GeV and multi–GeV data in terms of neutrino oscillations suggest for $|\Delta m^{2}|$ a value in the range $10^{-3} \div 10^{-2}$ eV², therefore matter effects are essentially negligible in the sub–GeV region, they can be relevant in the multi–GeV region if $|\Delta m^{2}|$ is close to the lower end of the above range, and are always significant for upward going muons.

2.2 Oscillation Probabilities

In the earth the composition remains always close to the value $Z/A \simeq 0.5$, but the density is not constant growing from a value of 2.7 g cm⁻³ at the surface to 12.5 g cm⁻³ close to the center. Therefore the effective oscillation parameters are not constant, and the flavor conversion probabilities must be obtained integrating the flavor evolution equation.

In fig. 3 we plot the survival probability of muon neutrinos as a function of the zenith angle, in the case of maximal mixing with tau, electron and sterile neutrinos. We are assuming that the neutrinos are created in a pure ν_{μ} state at the surface of the earth, and observed when they emerge again from the earth after traveling a distance $L = -2 R_{\oplus} \cos \theta_z$ ($R_{\oplus} \simeq 6371$ km is the earth radius). In each panel the curves correspond to the survival probability of a neutrino with energy $E_{\nu} = 20$, 40, 60 and 80 GeV if $\Delta m^2 = 5 \cdot 10^{-3} \text{ eV}^2$. The oscillation probability is a function of $E_{\nu}/\Delta m^2$ and the same curves describe the probabilities for different values of Δm^2 with a suitable rescaling of the values of the energy.

The upper panel shows the vacuum probabilities (appropriate for ν_{μ} – ν_{τ} mixing), that are sinusoidal curves of constant amplitude and oscillation length linearly growing with E_{ν} . In the middle and lower panel the survival probability for $\nu_{\mu} \leftrightarrow \nu_{e}$ and $\nu_{\mu} \leftrightarrow \nu_{s}$ oscillations are plotted. The most remarkable feature to note is the fact that for large E_{ν}

the curves take an approximately constant shape, with minima at fixed values of the zenith angle, but with an amplitude that decreases as E_{ν}^{-2} . In the case of $\nu_{\mu} \leftrightarrow \nu_{e}$ oscillations, the asymptotic shape of the transition probability has four maxima at $-\cos\theta_{z} \simeq 0.32$, 0.76, 0.90 and 1. In the case of oscillations into sterile neutrinos the large energy transition probability has two maxima, a broad one at $\cos\theta_{z} \simeq -0.45$ and a sharper and slightly higher one at $\cos\theta_{z} \simeq -0.90$ [24]. We can note that in the lower panel the curve labeled 20, that refers to a value $E_{\nu}/\Delta m^{2} = 4,000 \text{ GeV/eV}^{2}$, is still of an 'intermediate' shape, between the vacuum oscillation form and the asymptotic shape of the highest energies; in the $\nu_{\mu} \to \nu_{e}$ case where the matter effects are stronger ($V_{e\mu} = -2V_{\mu s}$) the corresponding curve has a shape closer to the asymptotic one.

To understand qualitatively these patterns in the oscillation probability it is useful to consider briefly propagation in a medium with constant density and composition. In this ideal case the oscillation probability can be written as:

$$P_{\nu_{\alpha}\to\nu_{\beta}} = \sin^2 2\theta \, \frac{\epsilon^2}{(1 - \epsilon \cos 2\theta)^2 + \epsilon^2 \sin^2 2\theta} \, \sin^2 \left[\frac{V_{\alpha\beta}L}{2} \sqrt{(1 - \epsilon \cos 2\theta)^2 + \epsilon^2 \sin^2 2\theta} \right] \,, \tag{7}$$

with $\epsilon = \zeta^{-1} = \Delta m^2/(2E_{\nu}V_{\alpha\beta})$. In the limit of large neutrino energy (that is for $\epsilon \to 0$) the transition probability becomes:

$$\lim_{E_{\nu \to \infty}} P_{\nu_{\alpha \to \nu_{\beta}}}^{\text{matter}} = \sin^2 2\theta \, \frac{|\Delta m^2|^2}{4 \, E_{\nu}^2 V_{\alpha\beta}^2} \, \sin^2 \left[\frac{V_{\alpha\beta} L}{2} \right] \,, \tag{8}$$

that oscillates with an asymptotic oscillation length $\ell_m^{\infty} = 2\pi/|V_{\alpha\beta}|$ independent from Δm^2 and E_{ν} , and only a function of the density and composition of the matter, and with an amplitude decreasing with the energy as E_{ν}^{-2} . These are qualitatively exactly the main features present in the middle and lower panels of fig. 3.

For a fixed value of L, the large energy limit of the oscillation probability in vacuum is readily obtained from eq. (1) as:

$$\lim_{E_{\nu} \to \infty} P_{\nu_{\mu} \to \nu_{\tau}} = \sin^2 2\theta \, \frac{|\Delta m^2|^2 L^2}{16 \, E_{\nu}^2} \,. \tag{9}$$

Comparing equations (8) and (9), we note that they differ because in the presence of matter the dependence on the distance L has a characteristic oscillating form instead of a quadratic increase. In the case of ν_{μ} – ν_{s} mixing the asymptotic oscillation length varies between 23,000 km (at the surface) and 5,300 km (at the earth's center), that corresponds to 3.65 and 0.81 earth radii, respectively; for ν_{μ} – ν_{e} , ℓ_{m}^{∞} is a factor of two shorter. This remarkable coincidence between the oscillation length of high energy ν_{μ} 's mixed with electron or sterile neutrinos when traversing the earth and the geometrical radius of our planet, generates a characteristic and observable deformation of the zenith angle distribution of the high energy neutrinos coming from below the horizon.

The considerations that we have outlined have been developed for constant density, but the qualitative conclusion that for large E_{ν} the curve of the oscillation probability as a function of zenith angle reaches an asymptotic shape remains valid also in the presence

of variable density and composition. In this more general case the shape is not exactly sinusoidal; for example one can see from fig. 3 that the maxima of the oscillation probability become narrower for neutrino trajectories that pass close to the center of the earth where the density is higher and the oscillation length shorter. We note that the density of the earth has a sharp discontinuity at a radius $r_c = 3493$ km, the boundary between the mantle and the core, where the density jumps from 5.5 to 9.9 g cm⁻³ [26]. A simple description of the density of the earth as composed of two layers of constant density with a discontinuity at r_c , is adequate to describe most of the features of the oscillation probabilities, as shown by the dashed curves [27] in the figures.

In fig. 4 we show survival probability curves for the case of a vacuum mixing angle with $\sin^2 2\theta = 0.7$. The upper panel is for $\nu_{\mu} \leftrightarrow \nu_{\tau}$ oscillations, the middle (lower) panel describe $\nu_{\mu} \leftrightarrow \nu_{s}$ ($\overline{\nu}_{\mu} \leftrightarrow \overline{\nu}_{s}$) oscillations for $\Delta m^2 > 0$. An MSW resonance is present for the antineutrinos when the condition $2 E_{\nu}(-V_{\mu s})/\Delta m^2 = \cos 2\theta$ is satisfied, while the mixing in matter of the neutrinos is always suppressed with respect to the vacuum case. In the case $\Delta m^2 < 0$ one should exchange the oscillation probabilities of neutrinos and antineutrinos. We can also note that asymptotically the shape of the oscillation probability as a function of zenith angle is the same as in the maximal mixing case, however at all energies the oscillation length of neutrinos (antineutrinos) is shorter (longer) than the maximal mixing case. The detection of the angular dependence of the oscillation probability is therefore more difficult if neutrino and antineutrino events are summed together.

3 Neutrino interactions in the detector

We discuss first the information that can be obtained from the events where the neutrinos interact in the detector via charged currents. In the presence of $\nu_{\mu} \leftrightarrow \nu_{\tau}$ or $\nu_{\mu} \leftrightarrow \nu_{s}$ oscillations, the rate of muon-like events is reduced, and its zenith angle and energy dependence is deformed. The absolute value of the theoretical prediction [29] has a large $(\sim 30\%)$ uncertainty that however to a good approximation affects in equal way the muon and electron (anti)neutrino fluxes, and therefore cancels in the analysis of the 'double ratio' $R = (N_{\mu}/N_e)_{DATA}/(N_{\mu}/N_e)_{MC}$. The Super-Kamiokande collaboration [2] in an exposure of 25.5 kton yrs, has measured $R = 0.610^{+0.029}_{-0.028} \pm 0.049$ for the sub–GeV sample and $R = 0.659^{+0.029}_{-0.058} \pm 0.053$ for the multi–GeV, showing a significant deviation from the expected value of 1. Fitting the energy and zenith angle dependence of the e-like and μ like events (the details are given in [30, 2]), the SK collaboration has calculated an allowed region at 90% C.L. in the ($|\Delta m^2|$, $\sin^2 2\theta$) plane for $\nu_{\mu}-\nu_{\tau}$ oscillations. It is in principle straightforward to repeat the analysis for the case of ν_{μ} – ν_{s} mixing. Recently Foot, Volkas and Yasuda [12, 17] have performed precisely this program, using the measurements of Rand of the angular distributions of μ -like and e-like events to recalculate the allowed region for the ν_{μ} - ν_{τ} hypothesis, estimating also the allowed regions for ν_{μ} - ν_{e} and ν_{μ} - ν_{s} mixing. The result obtained in [17] is that the regions allowed for ν_{μ} – ν_{τ} and ν_{μ} – ν_{s} oscillations are very similar, with the second one only slightly smaller, because the lowest values of $|\Delta m^2|$ allowed for oscillations into τ -neutrinos are excluded in the sterile case [31]. In this work we will not attempt to calculate again an allowed region in parameter space for ν_{μ} - ν_s mixing. We find that the result of [17] is qualitatively correct. For a more detailed analysis, one would need to have further informations on the detector acceptance and efficiency, and a knowledge of the bidimensional distribution in energy and direction of the events, that has not been published.

We would like instead to argue that the analysis of the zenith angle and energy dependence of the suppression of the μ -like events produced in the detector can distinguish between the hypotheses of oscillations into tau or sterile neutrinos only for $|\Delta m^2| \lesssim 4 \cdot 10^{-3} \text{ eV}^2$. This follows from the facts that: (a) the matter effects, depending on the quantity $E_{\nu} \rho/\Delta m^2$, vanish at low energy; (b) the atmospheric neutrino flux falls steeply with energy, and the rate of interactions of high energy neutrinos is small even for the large mass of Super-Kamiokande.

As an illustration in fig. 5 and 6 we show the zenith angle distributions of muons with momentum $p_{\mu} \geq 0.5$ (5.0) GeV produced inside the detector in charged current neutrino interactions, and the effects produced by $\nu_{\mu} \leftrightarrow \nu_{\tau}$ and $\nu_{\mu} \leftrightarrow \nu_{s}$ oscillations for two representative choices of oscillation parameters: maximal mixing and $\Delta m^{2} = 10^{-3} \text{ eV}^{2}$ (fig. 5) or $\Delta m^{2} = 5 \cdot 10^{-3} \text{ eV}^{2}$ (fig. 6). In order to generate these figures we have used a Montecarlo code based on the neutrino flux from Bartol [32] and the neutrino cross section as described in ref. [33]; to compute the oscillation probabilities we have also generated the neutrino production point according to the analytical approximations described in ref. [34]. The event rates calculated (for the position of the Gran Sasso underground laboratory) in the absence of oscillations are 82 and 10 events/(kton yr). No effects of detector efficiency and resolution have been included.

In the presence of oscillations the rate of muons events with up–going directions $(\cos \theta_z < 0)$ are strongly depleted. For the events with $p_\mu \ge 0.5$ (upper panels) the angle between the neutrino and the muon has a broad distribution with average $\langle \theta_{\mu\nu} \rangle = 26^{\circ}$ and this explains the loss of events also for downward–going directions. For the higher momentum events ($p_\mu \ge 5$ GeV, lower panels) the muon direction is more tightly correlated with the parent neutrino ($\langle \theta_{\mu\nu} \rangle = 6.5^{\circ}$), and the depletion of down–going events is much smaller.

The suppression of the rate in the case of ν_{μ} – ν_{s} oscillations is smaller than in the ν_{μ} – ν_{τ} case, because the effective mixing is reduced by matter effects. The difference between the two cases depends on the muon momentum considered (that is strongly correlated with the parent neutrino energy). For low muon momentum the oscillation probabilities of the two hypotheses are identical or very similar. With increasing momentum the matter effects become progressively more significant reducing the $\nu_{\mu} \leftrightarrow \nu_{s}$ oscillation probability. This different energy dependence of the oscillation probabilities is in fact the most easily detectable signature of the existence of mixing with sterile neutrinos.

The effect is also strongly dependent on the value of Δm^2 . In the case $\Delta m^2 = 10^{-3} \text{ eV}^2$ (fig. 5) the suppression N_{μ}/N_{μ}° of the muon rate with respect to the no-oscillation prediction, for the events with $p_{\mu} \geq 0.5$ GeV is 0.74 (0.78) in the cases of $\nu_{\mu}-\nu_{\tau}$ ($\nu_{\mu}-\nu_{s}$) mixing; for the higher momentum cut the suppression becomes 0.83 (0.94) for the two

cases, with a much larger difference. The angular dependence of the suppression is also different for oscillations into tau or sterile neutrinos [28].

For the higher value $\Delta m^2 = 5 \cdot 10^{-3} \text{ eV}^2$ (fig. 6) the suppression is nearly identical (0.689 and 0.695) in the case of the lower momentum muons and also for the higher momentum sample the difference between the two cases with suppressions of 0.74 and 0.78 is small.

To summarize this discussion in fig. 7 we plot the ratio N_{μ}/N_{μ}° of the muon rate to the prediction in the absence of oscillations, as a function of Δm^2 for the two different cuts in the muon momentum, $p_{\mu} \geq 0.5$ GeV or $p_{\mu} \geq 5.0$ GeV, both for maximal mixing (upper half of the figure) and for $\sin^2 2\theta = 0.80$ (lower half). The predictions for $\nu_{\mu} \leftrightarrow \nu_{\tau}$ oscillations are given by the full lines, those for oscillations into sterile neutrinos by dashed (dot–dashed) lines assuming $\Delta m^2 > 0$ ($\Delta m^2 < 0$). For very small $|\Delta m^2|$ the oscillation cannot develop and the ratio $N_{\mu}/N_{\mu}^{\circ} \simeq 1$; with increasing $|\Delta m^2|$ the ratio decreases monotonously, reaching asymptotically a value $1 - \frac{1}{2} \sin^2 2\theta$, corresponding to the averaging over rapid oscillations. Note that the region $|\Delta m^2| \sim 2 - 4 \cdot 10^{-3} \text{ eV}^2$ corresponds to a situation where most up–going (down–going) neutrinos do (do not) oscillate. From fig. 7 we can see that for sufficiently large $|\Delta m^2|$ the curves corresponding to the ν_{μ} – ν_{τ} and ν_{μ} – ν_{s} mixing become undistinguishable. Selecting higher momentum muons the difference between the two oscillation hypotheses remains significant until larger values of $|\Delta m^2|$, however the event sample available to study the effects becomes progressively smaller.

A larger number of high energy neutrino events is obtainable from the upward–going muon sample. In the remaining sections we discuss this class of events.

4 Upward-going muons

Muon neutrinos and antineutrinos can be detected indirectly observing the muons produced in CC interactions in the vicinity of the detector. In the presence of $\nu_{\mu} \rightarrow \nu_{x}$ oscillations the flux of ν -induced muons is suppressed, the energy spectrum is deformed and the angular distribution distorted. In essentially the entire region of ν -oscillations parameter space that is a solution for the atmospheric neutrino problem, the muon flux is modified in ways that are in principle observable with large area detectors. The neutrino energies that contribute to the muon flux extend up to ~ 1000 GeV, therefore the matter effects are important and allow in principle to distinguish between the ν_{μ} - ν_{τ} and ν_{μ} - ν_{s} hypotheses.

The ν -induced muon flux is measurable only in directions from below the horizon [35], therefore it is not possible to measure deviations from the up-down symmetry of the no-oscillation flux. The effects of oscillations can be studied only comparing the data with a Montecarlo calculation, based on assumptions about the primary cosmic ray flux, the properties of particle production in hadronic interactions with air-nuclei, the charged current neutrino cross section, and the properties of muon propagation. The theoretical uncertainties in the different elements of the calculation result in a systematic uncertainty

of $\sim 20\%$ for the absolute normalization of the flux. The energy and especially the zenith angle dependence of the flux can be calculated more reliably [36] and are useful probes of the existence of oscillations.

As an illustration of the effect of neutrino oscillations, in fig. 8 we show the flux of upward going muons above a minimum energy $E_{\min} = 1$ GeV plotted as a function of the zenith angle. The flux is calculated in the absence of oscillations, and for ν_{μ} - ν_{τ} and ν_{μ} - ν_{s} oscillation parameters corresponding to the SK 'test point' ($\Delta m^{2} = 5 \cdot 10^{-3} \text{ eV}^{2}$ and $\sin^2 2\theta = 1$). As a best estimate of the muon flux we have used the neutrino flux of Bartol [32], the cross sections described in [33] and the muon energy loss of [37]. The no-oscillation distribution has a maximum (minimum) for horizontal (vertical) muons, that reflects the larger flux of neutrinos for inclined directions. In reference [36] we have discussed in some detail the prediction of the upgoing muons zenith angle distribution and its theoretical uncertainties. Here we will concentrate on the shape of the distortion of the distribution produced by oscillations. In fig. 9, we have plotted the ratio between the oscillated and non-oscillated flux for different values of Δm^2 , always assuming maximal mixing. In the case of $\nu_{\mu} \leftrightarrow \nu_{\tau}$ oscillations the distortion factor varies smoothly and monotonously from a value close to unity for horizontal muons, to a maximum suppression for vertical muons. This behaviour can be easily understood: the neutrinos that generate the upward–going muons have a broad energy spectrum, with a shape that (in the absence of oscillations) changes only moderately for different zenith angles. For a fixed value of the zenith angle, the transition probability $P(\nu_{\mu} \to \nu_{\tau})$ is a function of the neutrino energy, for low E_{ν} it oscillates rapidly with an average value $\frac{1}{2}\sin^2 2\theta$, for large E_{ν} it decreases as L^2/E_{ν}^2 , and is negligibly small for $E_{\nu} \gg L |\Delta m^2| \simeq 2R_{\oplus} |\cos \theta_z| |\Delta m^2|$. With increasing $|\cos\theta_z|$ neutrinos of higher energy have a chance to oscillate and the muon flux is more suppressed.

In the case of oscillations with maximal mixing into sterile neutrinos, the suppression of the flux is smaller than in the corresponding vacuum case because the effective mixing in matter is reduced. The distortion factor does not depend monotonously on the zenith angle, but presents a structure with two minima at $\cos \theta_z \simeq -0.35$ and -0.9. The origin of this structure can be understood as a simple consequence of the considerations developed in the discussion of oscillation probabilities. The transition probability $P(\nu_{\mu} \to \nu_s)$ as a function of energy for a fixed zenith angle, is similar to the vacuum case for low E_{ν} . For larger E_{ν} it assumes the form discussed in section 2.2, developing a characteristic shape (see the lower panel in fig. 3) that after integration over all neutrino energies remains visible in fig. 9.

The detection of the structure in the distortion factor, present at $\cos \theta_z \simeq -0.9$ would be a clear and unambiguous experimental proof of the existence of mixing between muon and sterile neutrinos, but requires a large number of events. Easier to detect is perhaps the general trend of a suppression with respect to the no-oscillation expectation that becomes weaker going from $\cos \theta_z \simeq -0.3$ to $\cos \theta_z \simeq -0.8$, in constrast with the vacuum case.

The qualitative features of the distortion factors described above are present also selecting other energy intervals for the uwpard going muons. In fig. 10 we show the

distortion factor of the zenith angle distribution of upgoing muons in the interval $1 \le E_{\mu} \le 3$ GeV selected because it is in principle experimentally accessible, the muon energy being estimated from the measured range for stopping particles. The interval of parent neutrino energies that contributes to this flux is narrower, extending up to a neutrino energy of ~ 50 GeV. This can result in strong features in the angular distribution for Δm^2 smaller that $\sim 10^{-3}$ eV²; on the other hand for Δm^2 approaching 10^{-2} eV² the distortion factor rapidly reaches the constant value $1 - \frac{1}{2}\sin^2 2\theta$ both for vacuum and for matter oscillations.

In fig. 11 we show the distortion factors of the flux of muons with $E_{\mu} \geq 1$ GeV for $\Delta m^2 = 5 \cdot 10^{-3}$ eV² and $\sin^2 2\theta = 0.7$. In the case of vacuum oscillations the distortion factor for $\sin^2 2\theta < 1$ can be obtained from the result for maximal mixing simply as:

$$\langle P(\Delta m^2, \sin^2 2\theta) \rangle = \sin^2 2\theta \langle P(\Delta m^2, 1) \rangle$$
 (10)

where $\langle P \rangle = 1 - \phi_{\mu}/\phi_{\mu}^{\circ}$ is the fractional difference between the non oscillated and oscillated flux. In the presence of matter effects such a simple relation does not exist, and the dependence on the mixing angle in non trivial. The structure in the distortion factor is in general less visible in the case of non–maximal mixing. This is because the oscillation lengths of neutrinos and antineutrinos are different in the crucial region around the MSW resonance (see the curves labeled 'c' and 'd' in fig. 2) and this results in different angular patterns of the distortion for neutrinos and antineutrinos, as shown in fig. 4. It is important also to note that the sign of the mass difference, non observable in vacuum, is important in this case.

5 Upward-going muon data

Several detectors have collected data on neutrino-induced muons: Baksan [38], MACRO [39], Kamiokande [40], IMB [41], and Super-Kamiokande [2]. The situation at present is somewhat confused because of the poor agreement between different experiments, and between the data and theoretical expectations even after the inclusion of oscillations.

To compare theoretical predictions with experimental data we assume that the theoretical estimate of the flux is affected by systematic uncertainties that to a good approximation enter as a constant normalization factor without affecting the shape of the distribution [36]. We therefore define a χ^2 as:

$$\chi^2 = \min_{\alpha} \left\{ \sum_{j} \left(\frac{\phi_j - \alpha \, \phi_j^{th}}{\Delta \phi_j} \right)^2 + \left(\frac{1 - \alpha}{\Delta \alpha} \right)^2 \right\} \tag{11}$$

In eq. (11), the sum is over the number of bins in zenith angle (all experiments have been using 10 bins of equal width $\Delta\cos\theta_z=0.1$), ϕ_j and $\Delta\phi_j$ are the measured value of the flux in the bin and its error, ϕ_j^{th} is the calculated value and α is a normalization factor and $\Delta\alpha$ is the theoretical error, estimated as ~ 0.2 . The combination of experimental errors $(\Delta\phi_j$'s) and theoretical uncertainty $(\Delta\alpha)$ in the estimate of the χ^2 in eq. (11) cannot be

rigorously justified, but at least qualitatively has the desired features. Note that the limit $\Delta \alpha \to 0$ forces α to be 1, and corresponds to neglecting the theoretical uncertainties; the opposite limit $\Delta \alpha \to \infty$ takes into consideration only the shape of the zenith angle distribution.

5.1 Super-Kamiokande

The Super–Kamiokande collaboration [2] has presented data on through–going muons, that is tracks that enter in and exit from the detector, with a minimum path–length $L_{\min} = 7$ m. To compare with the experimental data we have calculated a muon flux as:

$$\phi^{th}(\cos \theta_z) = \frac{1}{A(L_{\min}, \theta_z)} \int_{E(L_{\min})}^{\infty} dE_{\mu} \, \frac{d\phi_{\mu}^{th}}{dE_{\mu}} (E_{\mu}, \cos \theta_z) [A(L_{\min}), \theta_z) - A(L(E_{\mu}), \theta_z)] \tag{12}$$

where $d\phi_{\mu}^{th}/dE_{\mu}$ is the flux of neutrino induced muons with energy E_{μ} and zenith angle θ_z , L(E) and E(L) are the muon range in water and its inverse function, and $A(L,\theta_z)$ is the projected area of the detector that corresponds to trajectories with internal pathlength longer than L. The factor $[A(L_{\min},\theta_z) - A(L(E_{\mu}),\theta_z)]$ weights the contribution of muons of energy E_{μ} to the flux, taking into account the fact that muons of low energy stopping in the detector should not be counted. Assuming for Super–Kamiokande the ideal geometry of a cylinder (with radius R=16.9 m and height H=36.2 m), a simple geometrical calculation gives:

$$A(L, \theta_z) = 2RH \sin \theta_z \sqrt{1 - x^2} + 2R^2 |\cos \theta_z| \left[\cos^{-1} x - 3x\sqrt{1 - x^2}\right] \Theta[L_{max}(\theta_z) - L],$$
(13)

with $x = L \sin \theta_z / 2R$ and $L_{\text{max}}(\theta_z) = \min [2R/\sin \theta_z, H/|\cos \theta_z|].$

Our calculation of the ν -induced muon flux is in excellent agreement with the one presented by the SK collaboration [2], indicating that our simple geometrical picture of the acceptance is a reasonable approximation. The main difference between our results and the theoretical curves presented by SK is a higher ($\sim 5\%$) absolute normalization of our estimate, probably due to the fact that we model the neutrino cross section including an explicit treatment of the quasi-elastic scattering and single-pion production [33].

An illustration of the effect of oscillations is shown in fig. 12, where we compare the SK data points with (i) a no-oscillation prediction (full line), (ii) $\nu_{\mu} \leftrightarrow \nu_{\tau}$ oscillations with $\sin^2 2\theta = 1$ and $\Delta m^2 = 10^{-2}$ eV² (dashed line), (iii) $\nu_{\mu} \leftrightarrow \nu_{s}$ oscillations with the same parameters (dot-dashed line). The three models have been calculated with the same theoretical input (ϕ_{ν} from Honda et al. [42], σ_{ν} as described in [33] with leading order PDF's from GRV [43]), and rescaled with factors $\alpha = 0.88$, 1.21 and 1.09. All three models give acceptable fits to the data, with χ^2 values of 12.8, 10.0 and 6.2. We can observe: (i) the no-oscillation hypothesis tends to be too flat, missing the data point for near-to-horizontal muons; (ii) the hypothesis of $\nu_{\mu} \leftrightarrow \nu_{\tau}$ oscillations with maximal mixing gives a high ratio between the horizontal and vertical flux, and in this hypothesis the best fit ($\chi^2 \simeq 8$) is obtained for $\sin^2 2\theta \simeq 0.70$; (iii) the hypothesis of $\nu_{\mu} \leftrightarrow \nu_{s}$ oscillations with maximal mixing gives a suprisingly good fit to the data. We would like to stress

the importance of the measurement of near–to–horizontal muons ($-0.1 < \cos \theta_z < 0$) in determining the results of the fits.

For the no–oscillation hypothesis, the $\chi^2=12.8$ has been computed assuming $\Delta\alpha=0.2$. Assuming instead $\Delta\alpha=0$ the χ^2 takes the value 20.4 (probability $2.6\cdot 10^{-2}$). Neglecting the absolute normalization (assuming $\Delta\alpha\to\infty$) the optimum α becomes 0.87 with χ^2 decreasing to 12.4; these numbers can be compared with the estimates: $\alpha=0.83$ and $\chi^2=12.7$ of the SK collaboration [2] done with the same neutrino flux [42]. Using the Bartol neutrino flux [32] we find a result that is 6.5% higher in absolute normalization with small differences in the angular distribution: for $\Delta\alpha=0.2$ the χ^2 for the no–oscillation hypothesis is 15.1.

The χ^2 resulting from fits to the data using the oscillation hypotheses (either $\nu_{\mu} \leftrightarrow \nu_{\tau}$ or $\nu_{\mu} \leftrightarrow \nu_{s}$) are presented in fig. 13 as a function of Δm^2 for $\sin^2 2\theta = 1$ and 0.8. It is interesting to note that the inclusion of neutrino oscillations, with parameters in the range suggested by the analysis of (semi–)contained events, does result in a better agreement between data and prediction. The best fit ($\chi^2 \simeq 6.1$) is obtained for $\nu_{\mu} \leftrightarrow \nu_{s}$ oscillations with $\Delta m^2 \simeq 1.4 \cdot 10^{-2} \,\mathrm{eV^2}$ and $\sin^2 2\theta \simeq 1$ (with $\alpha \simeq 1.12$). Assuming $\nu_{\mu} \leftrightarrow \nu_{\tau}$ oscillations the χ^2 is minimized ($\chi^2 \simeq 7.8$) for $\Delta m^2 \simeq 2.2 \cdot 10^{-2} \,\mathrm{eV^2}$ and $\sin^2 2\theta \simeq 0.7$ (with $\alpha = 1.18$).

Since our estimate of the theoretical error $\Delta\alpha\simeq0.2$ is rather arbitrary, we have repeated the fits for other choices of $\Delta\alpha$. The $\nu_{\mu}\to\nu_{s}$ hypothesis has always a lower χ^{2} , because it predicts a shape that is in closer agreement with the data and requires a normalization factor α closer to unity. Large values of Δm^{2} require a normalization factor considerably larger than unity, therefore an increased weight of the absolute normalization (i.e. smaller values of $\Delta\alpha$) lowers the best–fit values of Δm^{2} . The limiting case of $\Delta\alpha=0$ is illustrated in fig. 14. It may be noted that in this case, the range of parameters that minimize the χ^{2} for oscillations into sterile neutrinos is very similar to the one that fits the sub–GeV and multi–GeV SK data according to Foot et al. , as one can see comparing fig. 14 with fig. 12 in [17].

In summary, the SK data on upward going muons are consistent with the existence of neutrino oscillations, even if still inconclusive if taken by themselves. Considering the reduction of statistical errors expected with a longer exposure, future data should allow to distinguish the hypothesis of ν_{μ} – ν_{τ} and ν_{μ} – ν_{s} mixing.

Additional information on the existence of neutrino oscillations can be obtained from the analysis of neutrino induced muons that stop in the detector [41] (see also [13, 44, 36] for additional discussion). In fig. 15 we present predictions of the absolute rates and angular distributions of upgoing muons stopping in Super–Kamiokande. As discussed in previous works, in the presence of oscillations the flux of stopping muons is suppressed more strongly than the flux of through–going particles. The typical neutrino energies that produce stopping muons are similar to those that are the origin of multi–GeV events, and therefore matter effects have approximately the same importance. The suppression of the stopping flux and the distortion of the angular distribution depend on the type of oscillations only for small $|\Delta m^2|$.

5.2 Baksan and MACRO.

Data samples on upgoing muons with comparable statistics [45] have also been collected by other experiments. These data are difficult to describe both with and without oscillations, and also in poor agreement with each other [46, 2].

The Baksan and MACRO experiment have presented their results giving the muon flux above a threshold energy of 1 GeV correcting for the detector acceptance. We note that, as remarked in [36], the detectors do not have a sharp, angle independent threshold, and therefore the corrections are in principle model dependent.

We present in fig. 16 the data of the Baksan and MACRO detectors, together with fitted theoretical predictions. The fits are quite poor.

For Baksan the χ^2 of the no–oscillation hypothesis is $\chi^2 \simeq 26.6$ with a corresponding normalization factor $\alpha \simeq 0.95$. Including $\nu_{\mu} \leftrightarrow \nu_{\tau}$ ($\nu_{\mu} \leftrightarrow \nu_{s}$) oscillations does not result in a significantly better fit to the data: the minimum χ^2 is 25.7 (23.2) for $\Delta m^2 \simeq 1.0 \cdot 10^{-3} \text{ eV}^2$, $\sin^2 2\theta \simeq 0.70$ and $\alpha = 1.17$ ($\Delta m^2 \simeq -1.1 \cdot 10^{-3} \text{ eV}^2$, $\sin^2 2\theta \simeq 0.90$, $\alpha = 1.08$).

For MACRO the χ^2 for the no oscillation hypothesis (considering only statistical errors) is $\chi^2 \simeq 39$ (with $\alpha \simeq 0.70$). Including $\nu_{\mu} \leftrightarrow \nu_{\tau}$ ($\nu_{\mu} \leftrightarrow \nu_{s}$) oscillations the χ^2 is minimized ($\chi^2 = 30.2$ and 35.5) with the choice of parameters: $\Delta m^2 \simeq 1.5 \cdot 10^{-3} \text{ eV}^2$, $\sin^2 2\theta \simeq 1$, $\alpha = 0.97$ ($\Delta m^2 \simeq 1.5 \cdot 10^{-2} \text{ eV}^2$, $\sin^2 2\theta \simeq 1$, $\alpha = 1.02$). In the $\nu_{\mu} \leftrightarrow \nu_{\tau}$ hypothesis the χ^2 is reduced by 7 units, however given its large value the significance of the result is not clear.

The zenith angle distribution of the MACRO data shows some unexplained structure with a deficit for directions close to the vertical and an excess for $\cos\theta_z \simeq -(0.6\text{--}0.7)$. Liu and Smirnov [16] have suggested that this structure could be evidence for oscillations of muon into sterile neutrinos, observing that the qualitative features of the measured angular distribution are similar to those of the asymptotic form of the oscillation probability (see fig. 3). A more detailed calculation does not support this claim. In the case of ν_{μ} – ν_{s} mixing the matter effects do predict features like a reduction of the flux for $\cos\theta_z \sim -0.9$, however the amplitude of the effect is much smaller than what is measured by MACRO.

6 Conclusions

The simplest explanation for the atmospheric neutrino anomaly is the transition of muon neutrinos and antineutrinos into tau or sterile (anti)neutrinos. If the muon neutrinos are mixed with a singlet sterile state, the energy and zenith angle dependence of the oscillation probability is modified by matter effects. The differences between the cases of $\nu_{\mu}-\nu_{\tau}$ and $\nu_{\mu}-\nu_{s}$ mixing are important for $E_{\nu}/|\Delta m^{2}| \gtrsim 10^{3} \text{ GeV/eV}^{2}$. The two cases are distinguishable with high statistics studies of multi–GeV events, but only for the lower range of values of $|\Delta m^{2}|$ allowed by the analysis of (semi–)contained events. For larger $|\Delta m^{2}|$, the distinction will be possible through a detailed study of upgoing muons. The muon data available at present are of difficult interpretation, in that only the data obtained by the Super–Kamiokande collaboration are in agreement with theoretical expectations. Moreover, the Baksan and MACRO experimental data disagree with each other. The

SK data favour neutrino oscillations, albeit with low statistical significance; both $\nu_{\mu} \leftrightarrow \nu_{s}$ (with slightly better agreement) and $\nu_{\mu} \leftrightarrow \nu_{\tau}$ oscillations provide good fits. We can expect that forthcoming additional data will clarify the situation and allow to identify the right solution.

Acknowledgments

The authors wish to acknowledge useful discussions with S.P.Mikheyev.

References

- [1] K.S. Hirata et al., Phys.Lett. B 205, 416 (1988) and ibid. 280, 146 (1992);
 - Y. Fukuda *et al.*, Phys.Lett. B **335**, 237 (1994);
 - D. Casper *et al.*, Phys.Rev.Lett. **66**, 2561 (1991); R. Becker–Szendy *et al.*, Phys.Rev.
 - D 46, 3720 (1992);
 - T. Kafka, Soudan–2 collaboration, Proceedings of TAUP97;
 - Y. Fukuda *et al.*, Super–Kamiokande collaboration, hep-ex/9803006, submitted to Phys.Lett.
- [2] E. Kearns, Proceedings of TAUP97, hep-ex/9803007.
- [3] see for example V. Berezinsky, Invited lecture at 25^{th} ICRC, Durban, July 28 August 8, 1997, astro-ph/9710126.
- [4] C. Athanassopoulos et al, (LSND Collaboration) Phys. Rev. Lett. **77**, 3082 (1996); nucl-ex/9706006; nucl-ex/9709006.
- [5] There have been several attempts to reconcile all detected anomalies with a scheme involving only three neutrino flavors, suggesting for example that $\Delta m_{LSND}^2 = \Delta m_{atm}^2$ [6, 7], or that $\Delta m_{\odot}^2 = \Delta m_{atm}^2$ [8]. The first scenario predicts the absence of a zenith angle dependence of the atmospheric neutrino anomaly, the second one predicts a constant suppression for all solar neutrino experiments and, since the atmospheric neutrino anomaly is essentially due to $\nu_{\mu} \leftrightarrow \nu_{e}$ in this case, a positive signal for the Chooz experiment [9]; therefore both scenarios are currently not supported by the data.
- [6] C.Y.Cardall and G M.Fuller, Phys. Rev. D 53, 4421 (1996).
- [7] G.L. Fogli, E. Lisi, D. Montanino and G. Scioscia, Phys. Rev. D 56, 4365 (1997).
- [8] A. Acker and S. Pakvasa, Phys. Lett. B **397**, 209 (1997).
- [9] Chooz collaboration: M. Apollonio et al., hep-ex/9711002.
- [10] The current value for the number of standard light neutrinos is $N_{\nu} = 2.995 \pm 0.061$, see LEP Electroweak Working Group, CERN/PPE/95–172.

- [11] M.C. Gonzalez-Garcia, H. Nunokawa, O.L.G. Peres, T. Stanev and J.W.F. Valle, hep-ph/9801368.
- [12] R. Foot, R. R. Volkas and O. Yasuda, hep-ph/9802287.
- [13] E. Akhmedov, P. Lipari, and M. Lusignoli, Phys. Lett. B 300, 128 (1993).
- [14] R. Foot, Mod. Phys. Lett. A 9, 169 (1994);
 R. Foot and R.R. Volkas, Phys. Rev. D 52, 6595 (1995);
 S.M. Bilenky, C. Giunti and W. Grimus, Proc. of Neutrino 96, Helsinki, June 1996, edited by K. Enqvist et al., p. 174.
- [15] F. Vissani and A.Yu. Smirnov, hep-ph/9710565.
- [16] Q.Y. Liu and A.Yu. Smirnov, hep-ph/9712493.
- [17] R. Foot, R.R. Volkas and O. Yasuda, hep-ph/9801431.
- [18] A. Dolgov, Sov. J. Nucl. Phys. 33, 700 (1981);
 R. Barbieri and A. Dolgov, Phys. Lett. B 237, 440 (1990) and Nucl. Phys. B 349, 743 (1991);
 K. Enqvist, K. Kainulainen and M. Thomson, Phys. Rev. Lett. 68, 744 (1992) and Nucl. Phys. B 373, 498 (1992);
 J. Cline, Phys. Rev. Lett. 68, 3137 (1992);
 X. Shi, D. N. Schramm and B. D. Fields, Phys. Rev. D 48, 2568 (1993).
- [19] D.Schramm and M.Turner, Rev. Mod. Phys. **70**, 303 (1998).
- [20] R.Foot and R.Volkas, Phys. Rev. D 55, 5147 (1997);
 R.Foot and R.Volkas, Phys. Rev. D 56, 6653 (1997).
- [21] S.J. Barish *et al.*, Phys.Rev.D **19**, 2521 (1979).
- [22] G.L. Fogli and G. Nardulli, Nucl. Phys. B **160**, 116 (1979).
- [23] L. Wolfenstein, Phys. Rev. D 17, 2369 (1978);
 S.P. Mikheyev and A.Yu. Smirnov, Yad. Fiz. 42, 1441 (1985) [Sov.J.Nucl.Phys. 42, 913 (1985)].
- [24] The enhancement of the amplitude of oscillations at $\cos \theta_z \simeq 0.9$, in the case of ν_{μ} – ν_s mixing, can be understood [16] as a case of 'parametric resonance' [25].
- [25] E. Akhmedov, Yad.Fiz. 47, 475 (1988);
 P.I. Krastev and A.Y. Smirnov, Phys. Lett. B 226, 341 (1989).
- [26] F.D. Stacey, "Physics of the earth", Wiley, New York, 1969.

- [27] The dashed curves in fig. 3 and 4 are calculated assuming a constant density in the core and mantle of the earth $\langle \rho_c(\theta_z) \rangle$ and $\langle \rho_m(\theta_z) \rangle$, calculated averaging the density along a trajectory of zenith angle θ_z .
- [28] Note in the lower panels of fig. 5 and 6 that the suppression factor for $\nu_{\mu} \rightarrow \nu_{s}$ transitions, if studied in great detail shows a complex dependence on the zenith angle that can be compared with the oscillation probability curves in fig. 3.
- [29] T. K. Gaisser, M. Honda, K. Kasahara, H. Lee, S. Midorikawa, V. Naumov, T. Stanev, Phys.Rev. D 54, 5578 (1996).
- [30] Y. Fukuda et al., Phys.Lett. B **335**, 237 (1994).
- [31] We note that in [17] the authors have considered only the case of positive Δm^2 . Matter effects allow to distinguish the case of positive and negative squared mass differences, and the allowed region for $\Delta m^2 < 0$ is somewhat larger than in the other case, because of the MSW resonance present for the neutrinos.
- [32] V. Agrawal, T. K. Gaisser, P. Lipari, and T. Stanev, Phys. Rev. D 53 1314, (1996).
- [33] P. Lipari, M. Lusignoli, and F. Sartogo, Phys.Rev.Lett. 74, 4384 (1995).
- [34] T.K. Gaisser and Todor Stanev, Phys. Rev. D 57, 1977 (1998).
- [35] The flux of ν -induced muons is larger than the flux of atmospheric muons for line of sights shielded by a column density larger than $\sim 10^6$ g cm⁻². In the upper hemisphere this condition is satisfied at most in a small solid angle for the deepest detectors.
- [36] P. Lipari and M. Lusignoli, hep-ph/9712278, Phys. Rev. D 57, 3842R (1998).
- [37] W. Lohmann, R. Kopp & R. Voss, CERN Yellow Report No. EP/85-03.
- [38] Baksan Collaboration: M. M. Boliev et al., ICRC '95, Rome, Vol 1, p. 686; ibidem, p. 722.
- [39] MACRO Collaboration: S. Ahlen et al., Phys. Lett. B 357, 481 (1995); F. Ronga et al., in Neutrino '96, Proceedings of the 17th Conference on Neutrino Physics and Astrophysics, Helsinki, 1996.
- [40] Kamiokande Collaboration: A. Suzuki *et al.* in Proceedings of 7th International Workshop on Neutrino Telescopes, Venice, 1996, edited by M. Baldo Ceolin p. 263.
- [41] IMB Collaboration: R. Becker-Szendy et al., Phys. Rev. Lett. 69, 1010 (1992);
 D. W. Casper, in Proceedings of 3rd International Workshop on Neutrino Telescopes, Venice, 1991, edited by M. Baldo Ceolin p. 213.

- [42] M. Honda, T. Kajita, K. Kasahara, and S. Midorikawa, Phys. Rev. D 52, 4985 (1995);
- [43] M. Gluck, E. Reya, and A. Vogt, Z.Phys. C 67, 433 (1995).
- [44] W. Frati, T. K. Gaisser, A. K. Mann, and T. Stanev, Phys. Rev. D 48, 1140 (1993).
- [45] The acceptance for the muon flux increases with the area (as opposed to the volume) of the detector: SK does not dominate the other experiments as for the contained neutrino events.
- [46] G.L. Fogli, E. Lisi and A. Marrone, preprint BARI-TH-280-97, hep-ph/9708213.

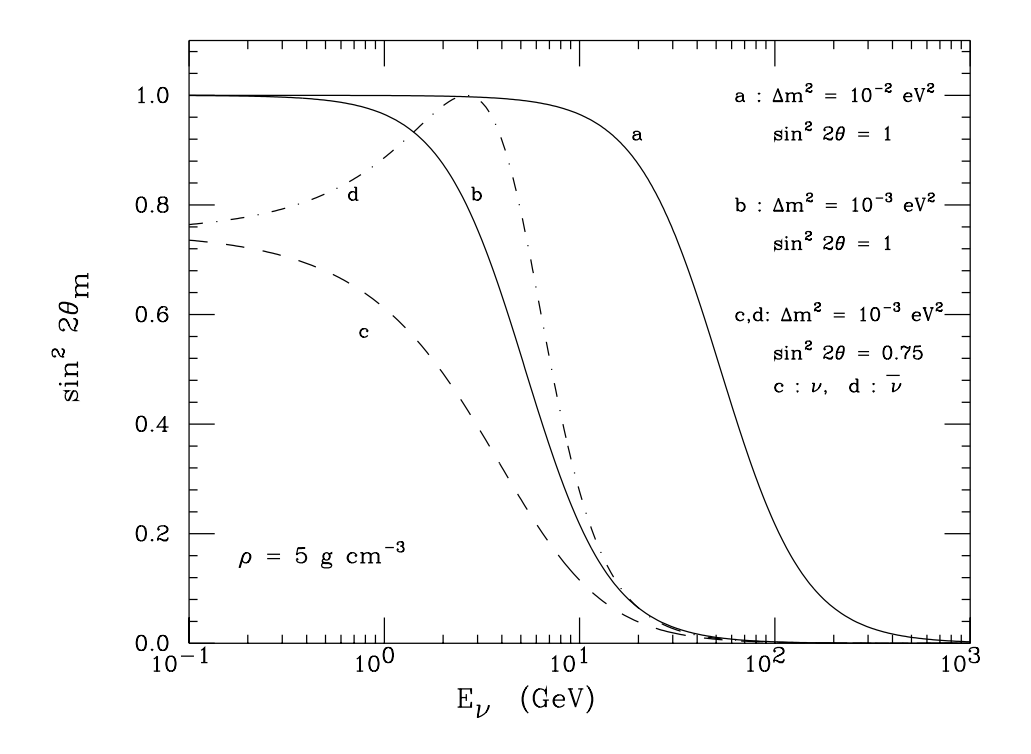


Figure 1: Effective mixing parameter for ν_{μ} – ν_{s} oscillations in matter with constant density $\rho=5~{\rm g~cm^{-3}}$ and neutron fraction 0.5.

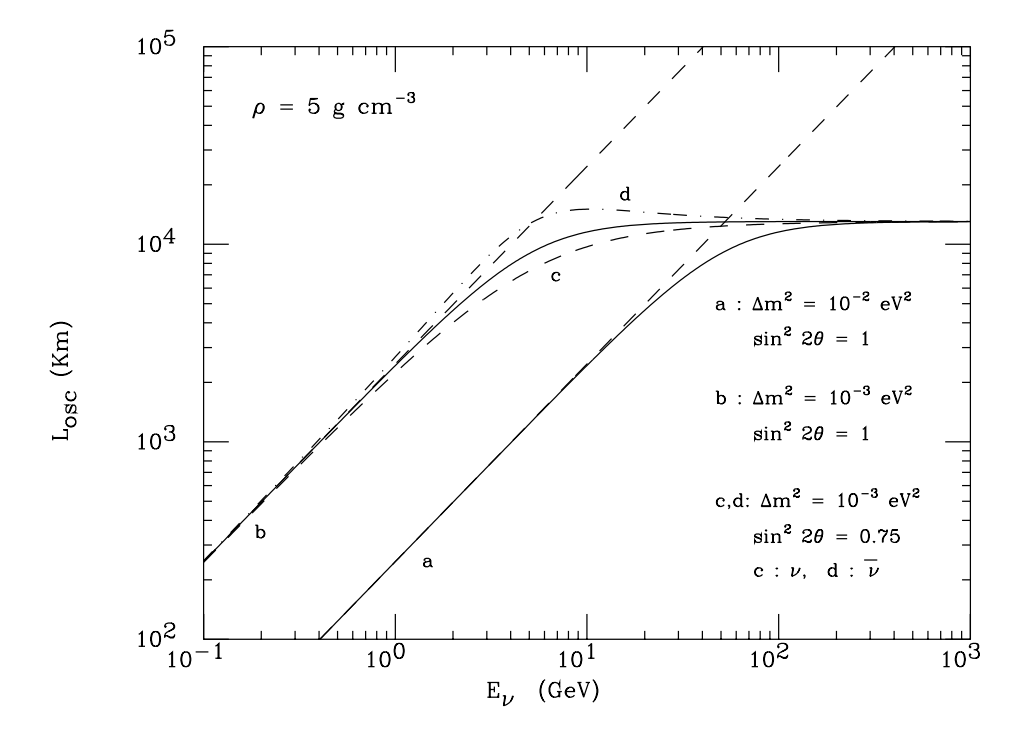


Figure 2: Oscillation length in matter.

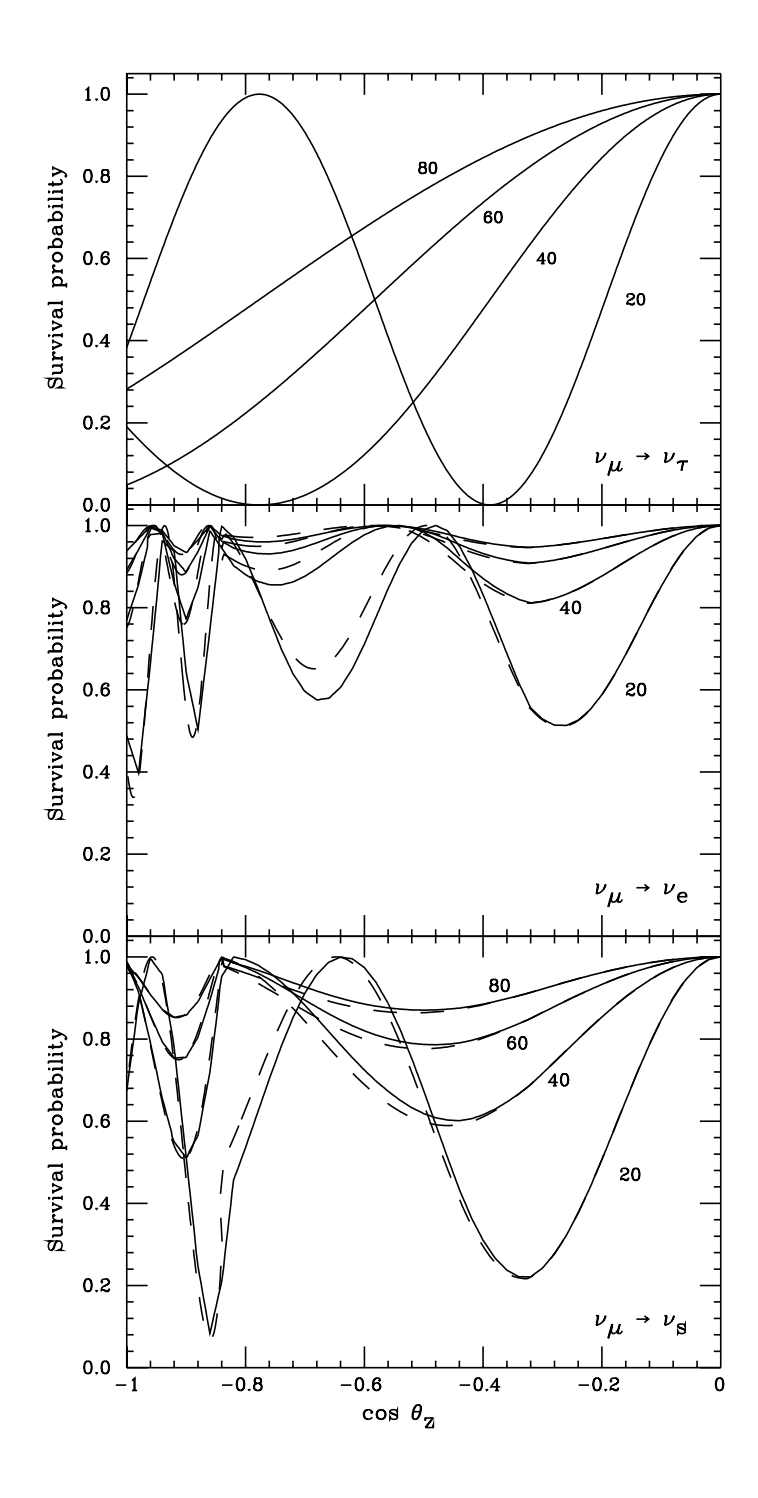


Figure 3: Survival probability $P(\nu_{\mu} \to \nu_{\mu})$ as a function of the zenith angle in the case of maximal mixing of ν_{μ} with ν_{τ} (upper panel), ν_{e} (middle panel) and ν_{s} (lower panel). For $|\Delta m^{2}| = 5 \cdot 10^{-3} \text{ eV}^{2}$ the curves correspond to neutrino energies 20, 40, 60 and 80 GeV. The dashed curves are calculated with the approximation of constant average densities in the mantle and in the core of the earth [27].

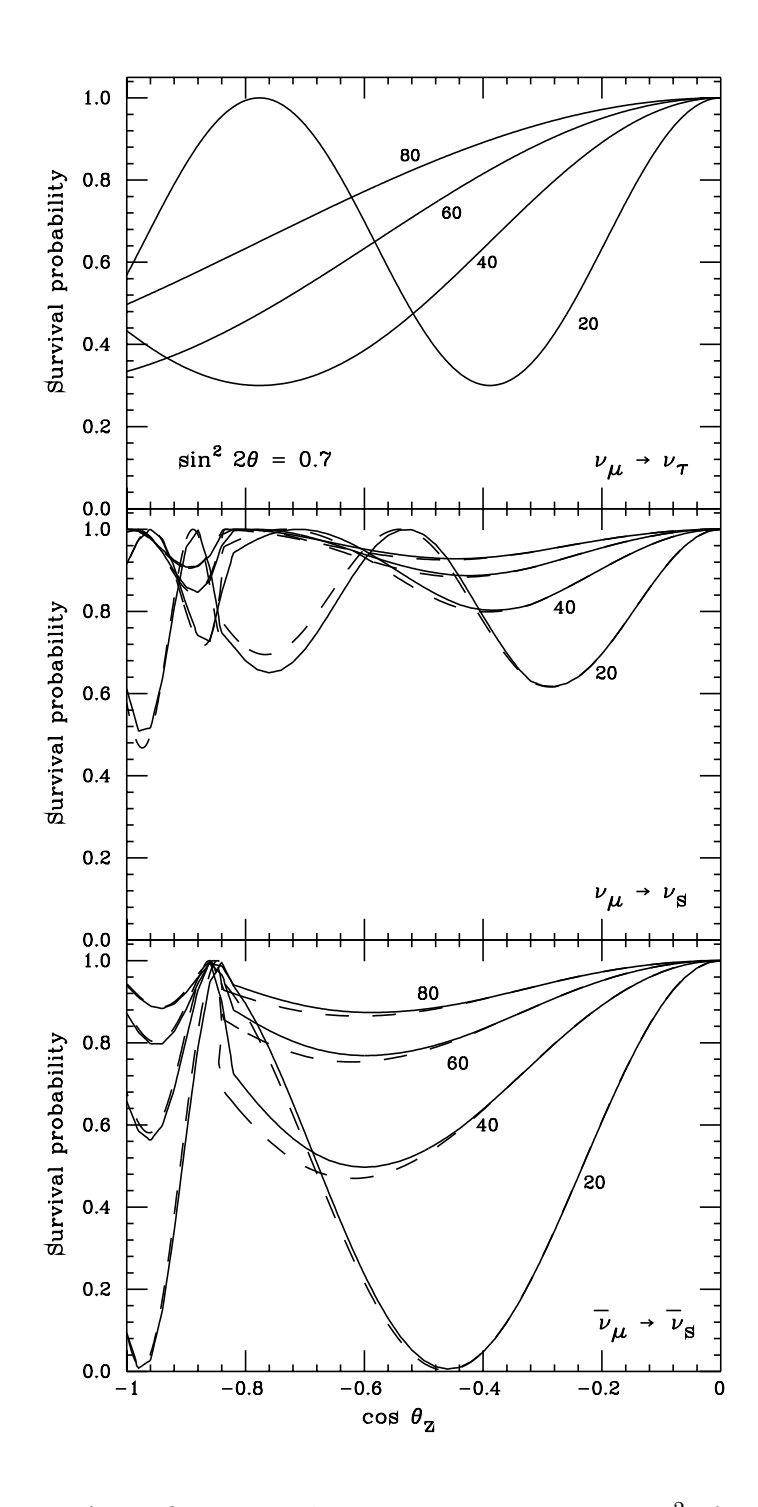


Figure 4: As in figure 3. The mixing parameter is $\sin^2 2\theta = 0.7$.

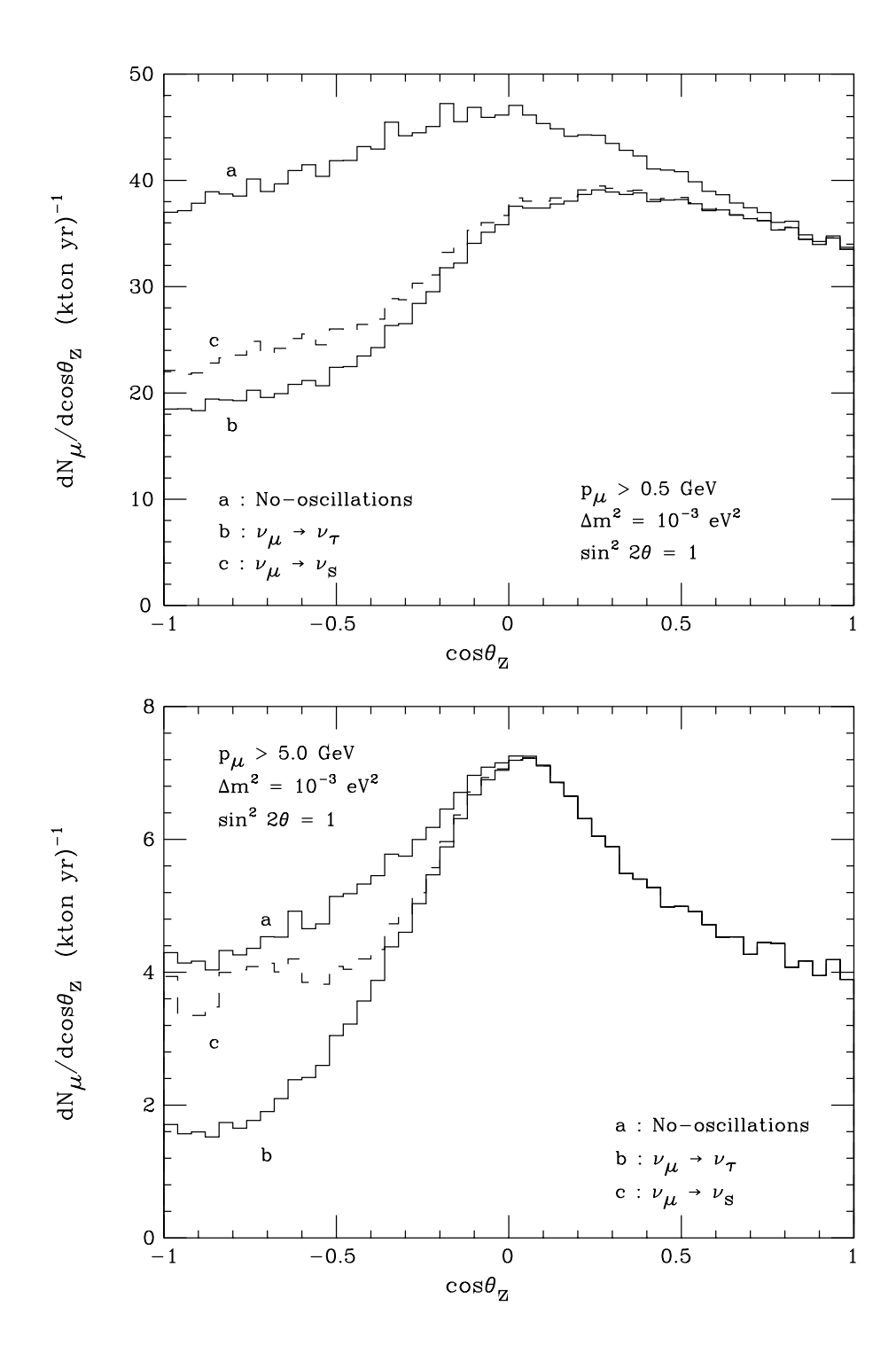


Figure 5: Upper panel: Angular distribution of the muon events with $p_{\mu} \geq 0.5$ GeV, in the absence of oscillations (histogram a), and in the presence of oscillations with $\Delta m^2 = 10^{-3} \text{ eV}^2$ and maximal ν_{μ} – ν_{τ} (b) or ν_{μ} – ν_{s} (c) mixing. Lower panel: the same, with $p_{\mu} \geq 5.0$ GeV.

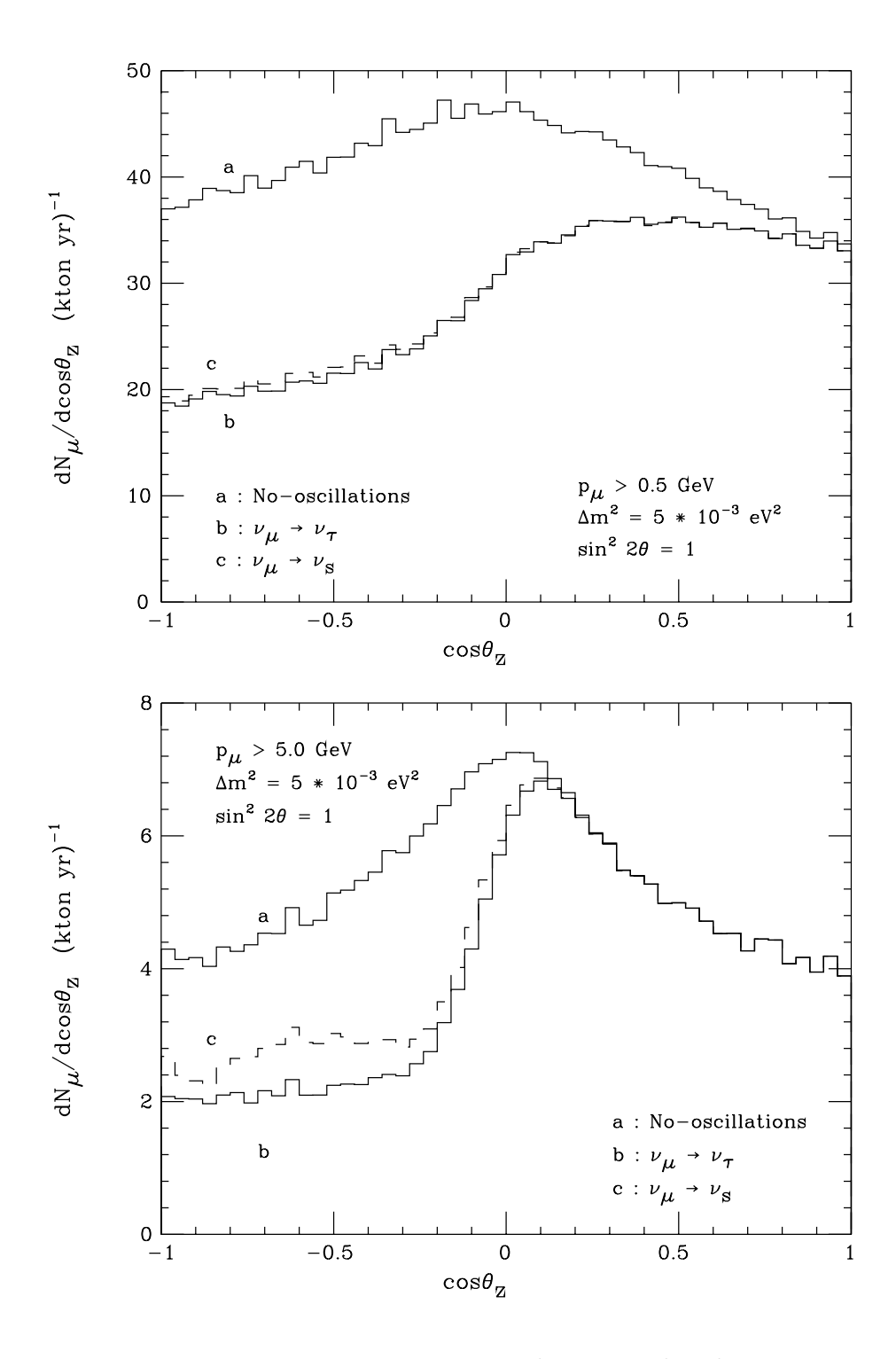


Figure 6: As in fig. 5, with $\Delta m^2 = 5 \cdot 10^{-3} \text{ eV}^2$.

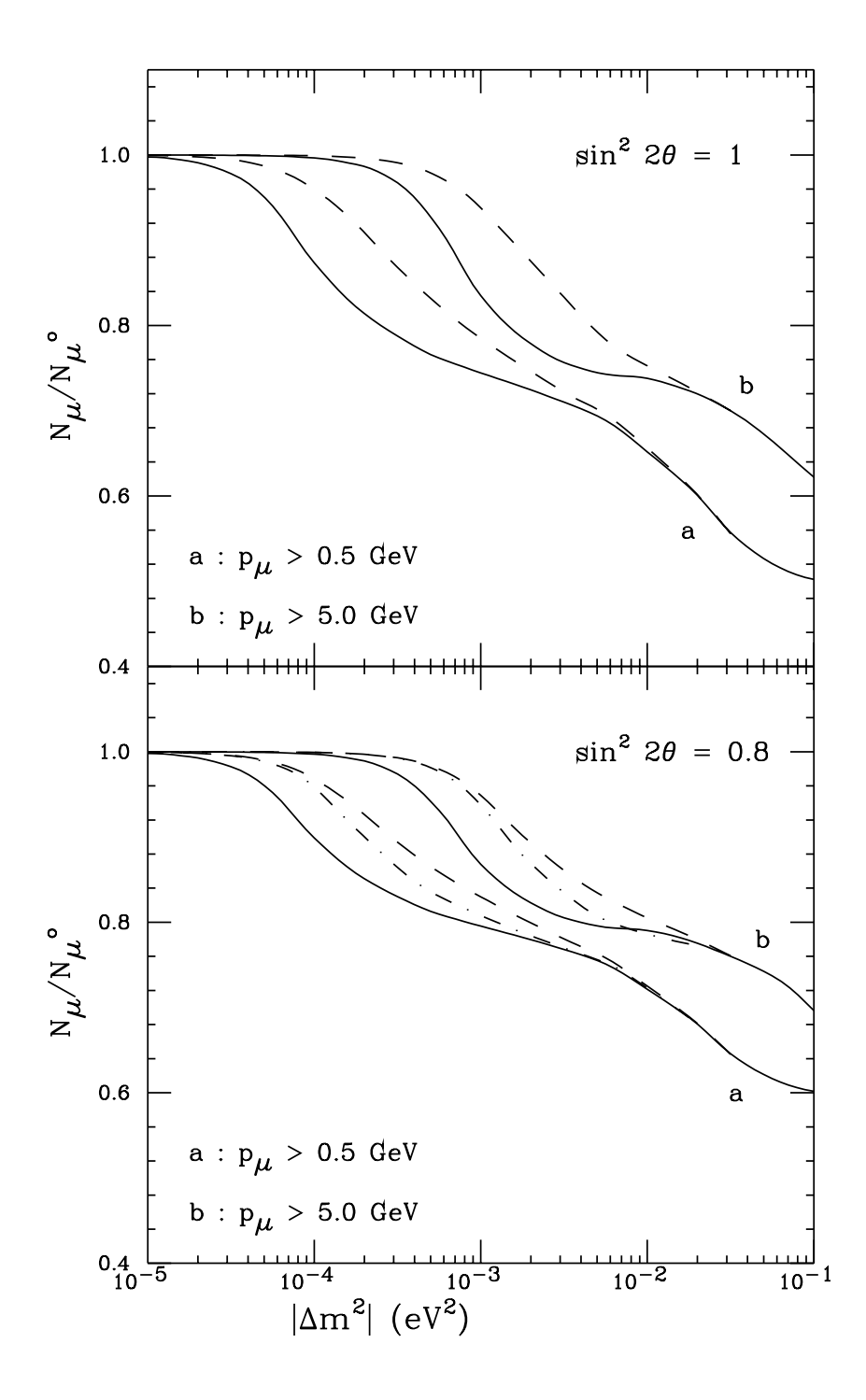


Figure 7: Ratio of the rate of muon events to the no-oscillation case as a function of Δm^2 , for two choices of the minimum muon momentum. The upper (lower) panel is calculated for $\sin^2 2\theta = 1$ (0.8). The solid (dashed) curves are for $\nu_{\mu} - \nu_{\tau}$ ($\nu_{\mu} - \nu_{s}$) mixing. In the lower panel the dot-dashed curve describes $\nu_{\mu} - \nu_{s}$ mixing with $\Delta m^2 < 0$.

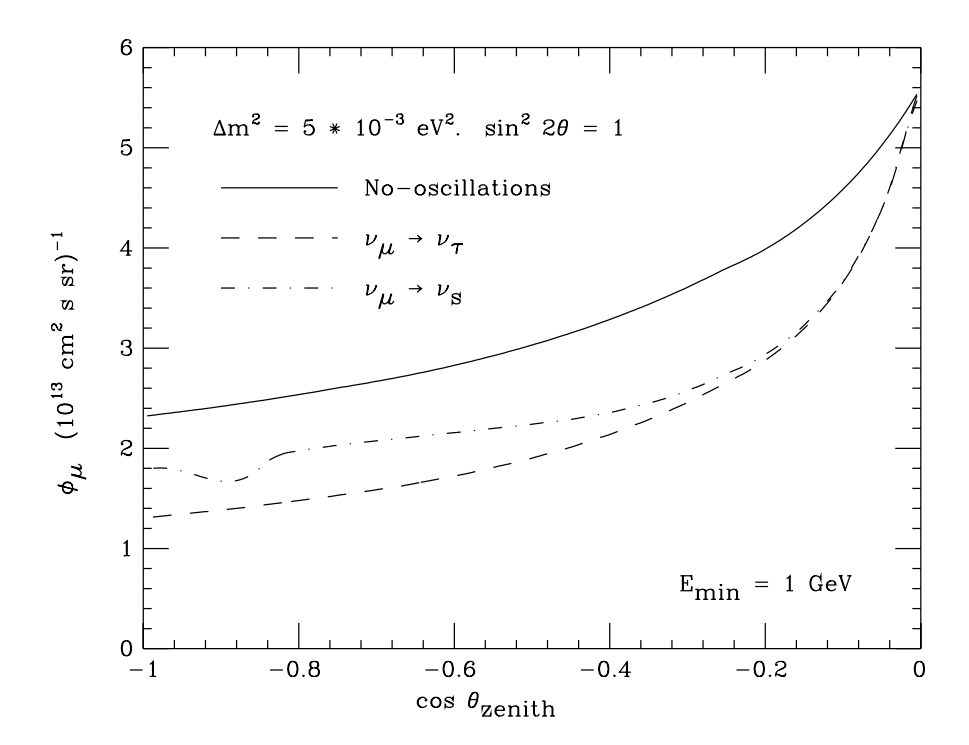


Figure 8: Upward–going muon flux as a function of zenith angle (with $E_{\rm min}=1~{\rm GeV}$), in the absence of oscillations (solid line), and for maximal mixing and $\Delta m^2=5\cdot 10^{-3}~{\rm eV^2}$ in the cases of $\nu_{\mu}\to\nu_{\tau}$ (dashes) and $\nu_{\mu}\to\nu_{s}$ (dot–dashes).

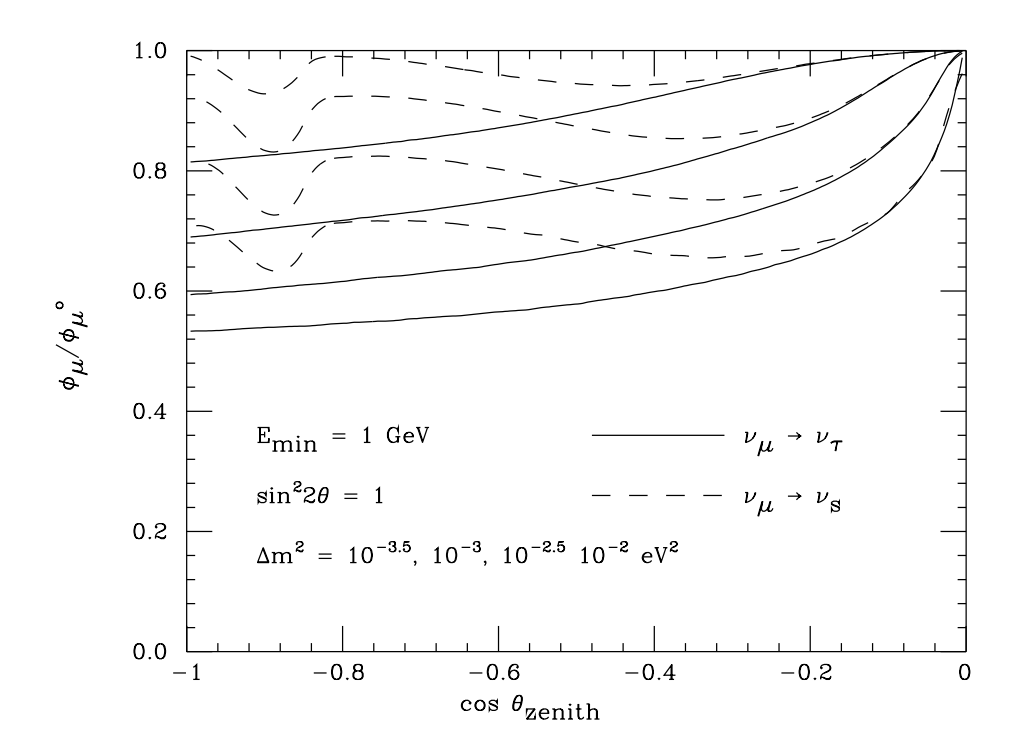


Figure 9: Ratio between the upward–going muon flux ($E_{\mu} \geq 1$ GeV), and the no-oscillation prediction for maximal mixing and (starting from the highest line) $\Delta m^2 = 10^{-3.5}$, 10^{-3} , $10^{-2.5}$ and 10^{-2} eV². The solid (dashed) lines are for ν_{μ} – ν_{τ} (ν_{μ} – ν_{s}) mixing.

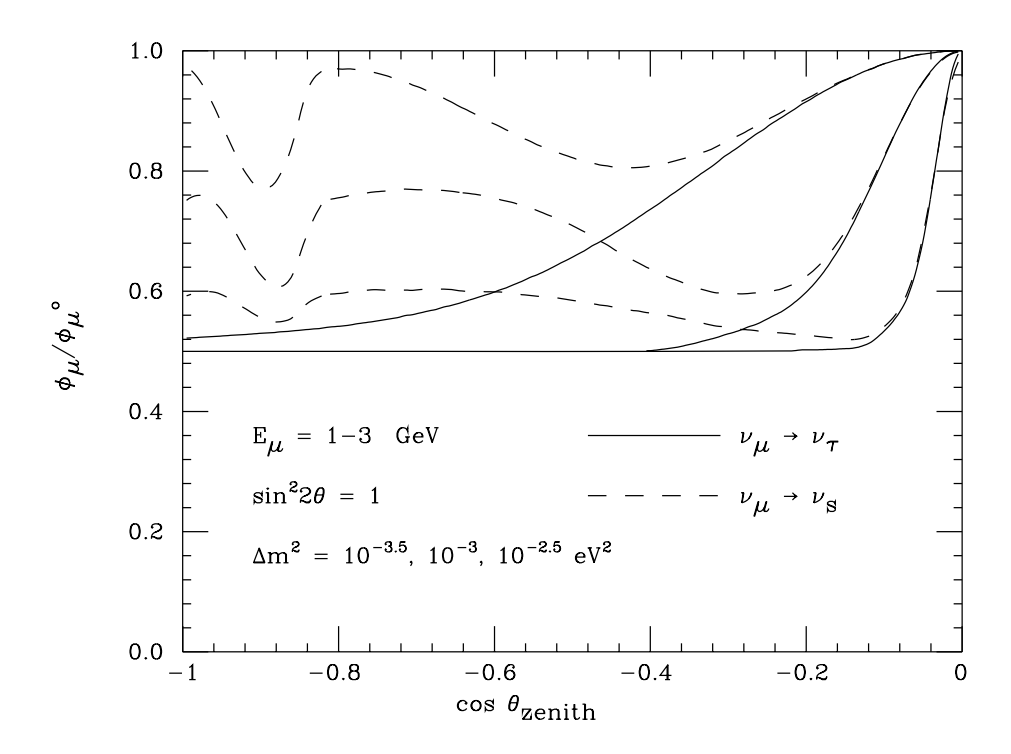


Figure 10: As in fig. 9, with the upward going muon flux calculated in the energy interval $1 \le E_{\mu} \le 3$ GeV.

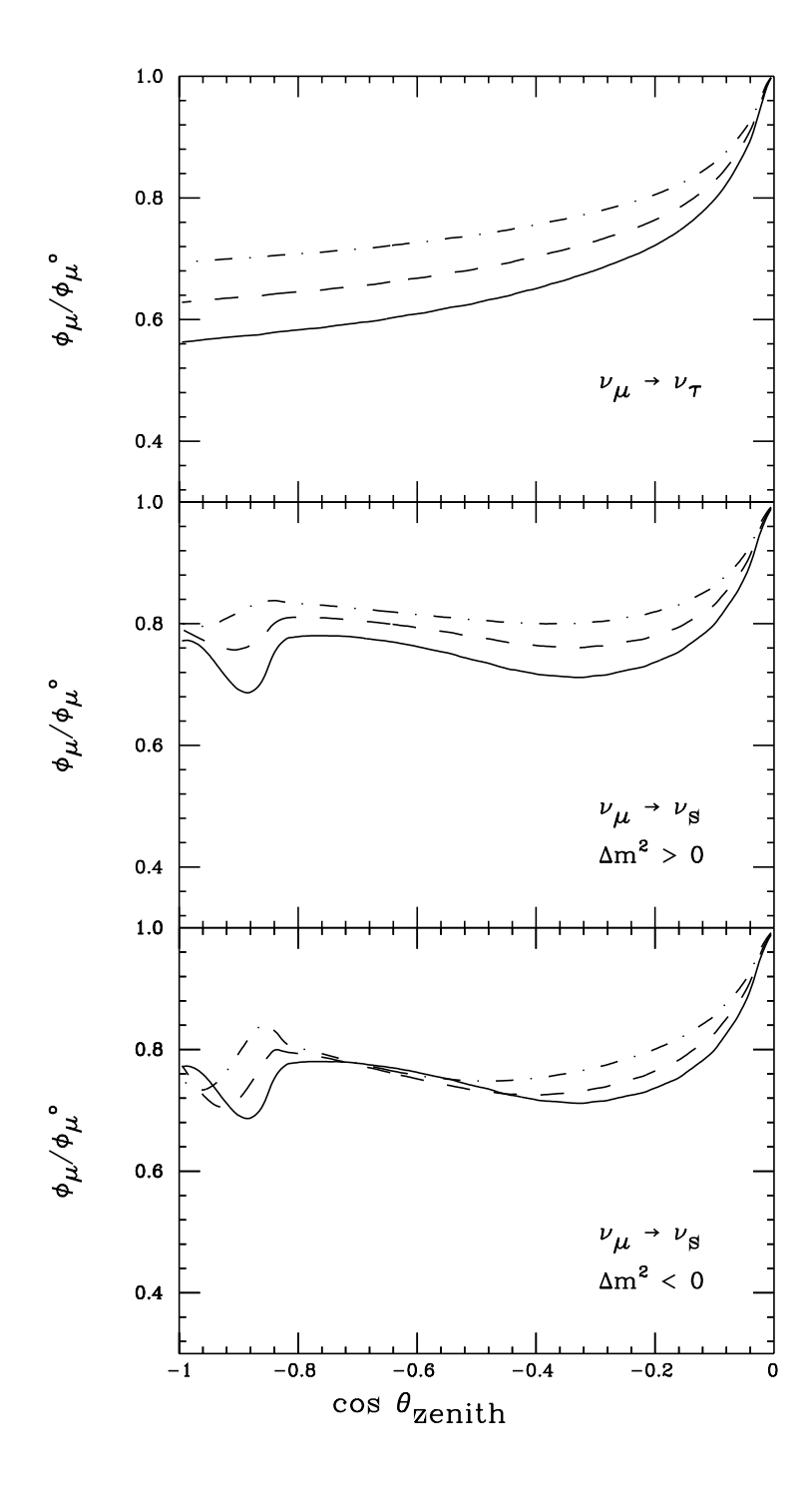


Figure 11: Ratio between the upward–going muon flux ($E_{\mu} \geq 1$ GeV), and the no-oscillation prediction for $|\Delta m^2| = 5 \cdot 10^{-3} \text{ eV}^2$ and $\sin^2 2\theta = 1$ (full curves), 0.9 (dashed) and 0.8 (dot-dashed). The upper panel is for ν_{μ} – ν_{τ} mixing, the middle (lower) panel for ν_{μ} – ν_{s} mixing and positive (negative) Δm^2 .

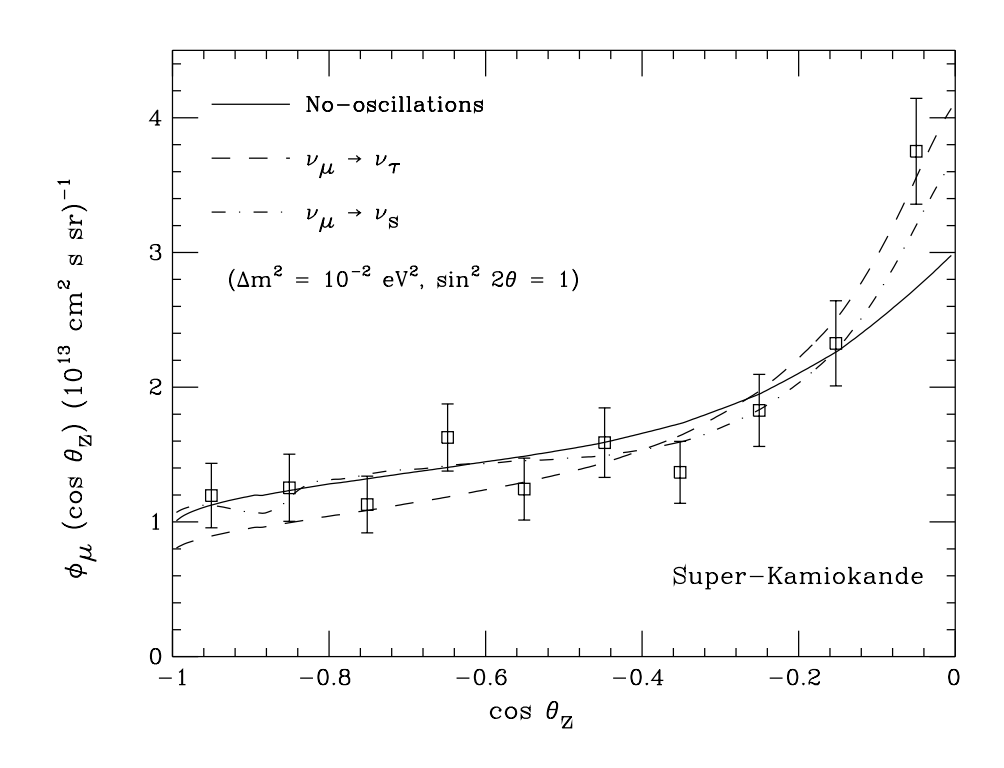


Figure 12: Flux of through–going upward going muons measured by Super–Kamiokande [2], compared with theoretical predictions with and without oscillations (see text)

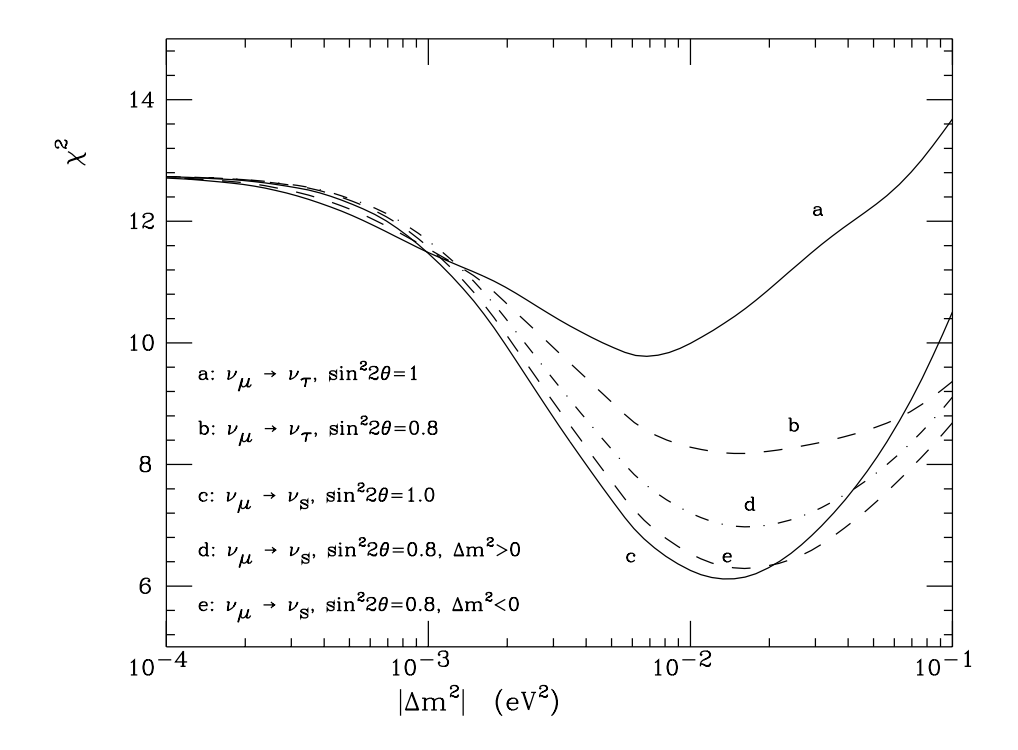


Figure 13: χ^2 of fits to the upward–going muons data of Super–Kamiokande calculated according to eq. 11 plotted as a function of Δm^2 , for $\sin^2 2\theta = 1$ and 0.8 assuming $\nu_\mu - \nu_\tau$ and $\nu_\mu - \nu_s$ mixing. The uncertainty $\Delta \alpha$ on the absolute normalization is 0.2.

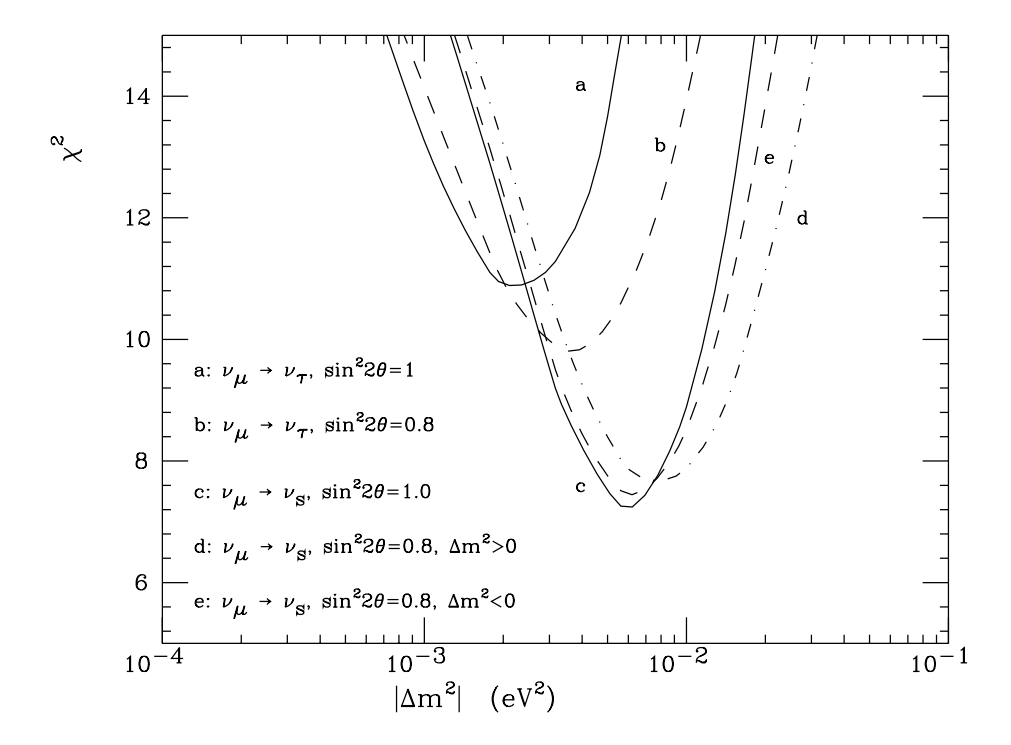


Figure 14: χ^2 of fits to the SK upgoing muons (as in fig. 13) calculated with a fixed normalization ($\alpha=1$).

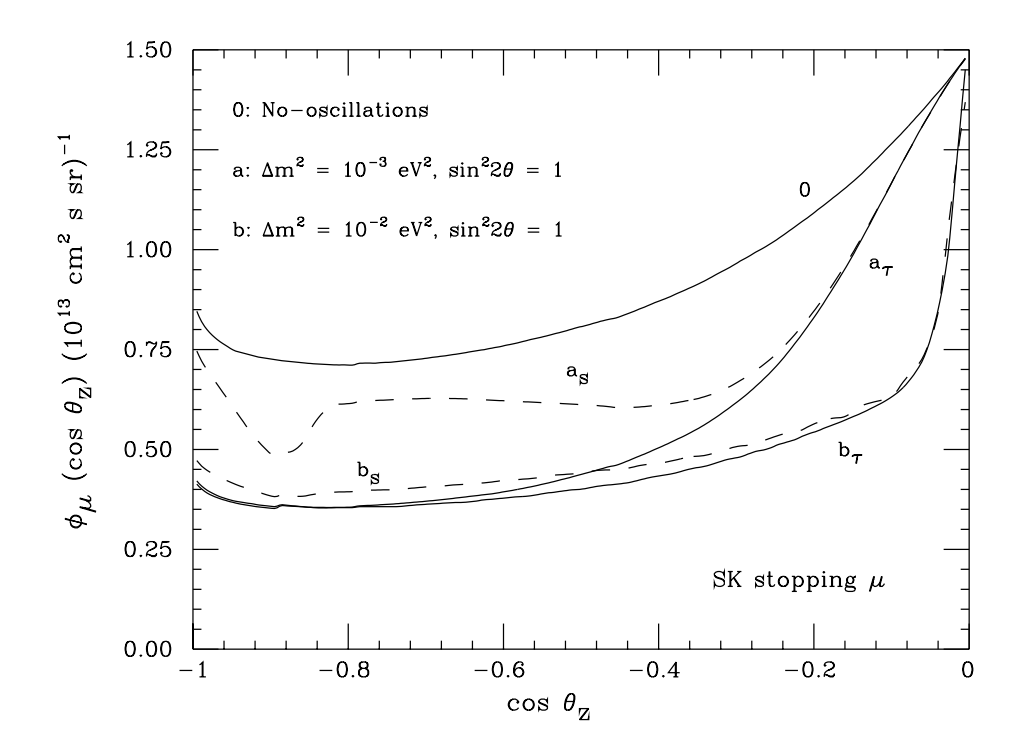


Figure 15: Predictions of the rate and angular distribution of stopping muons in SK, in the absence (and presence) of oscillations. The subscript τ (s) indicates ν_{μ} – ν_{τ} (ν_{μ} – ν_{s}) mixing.

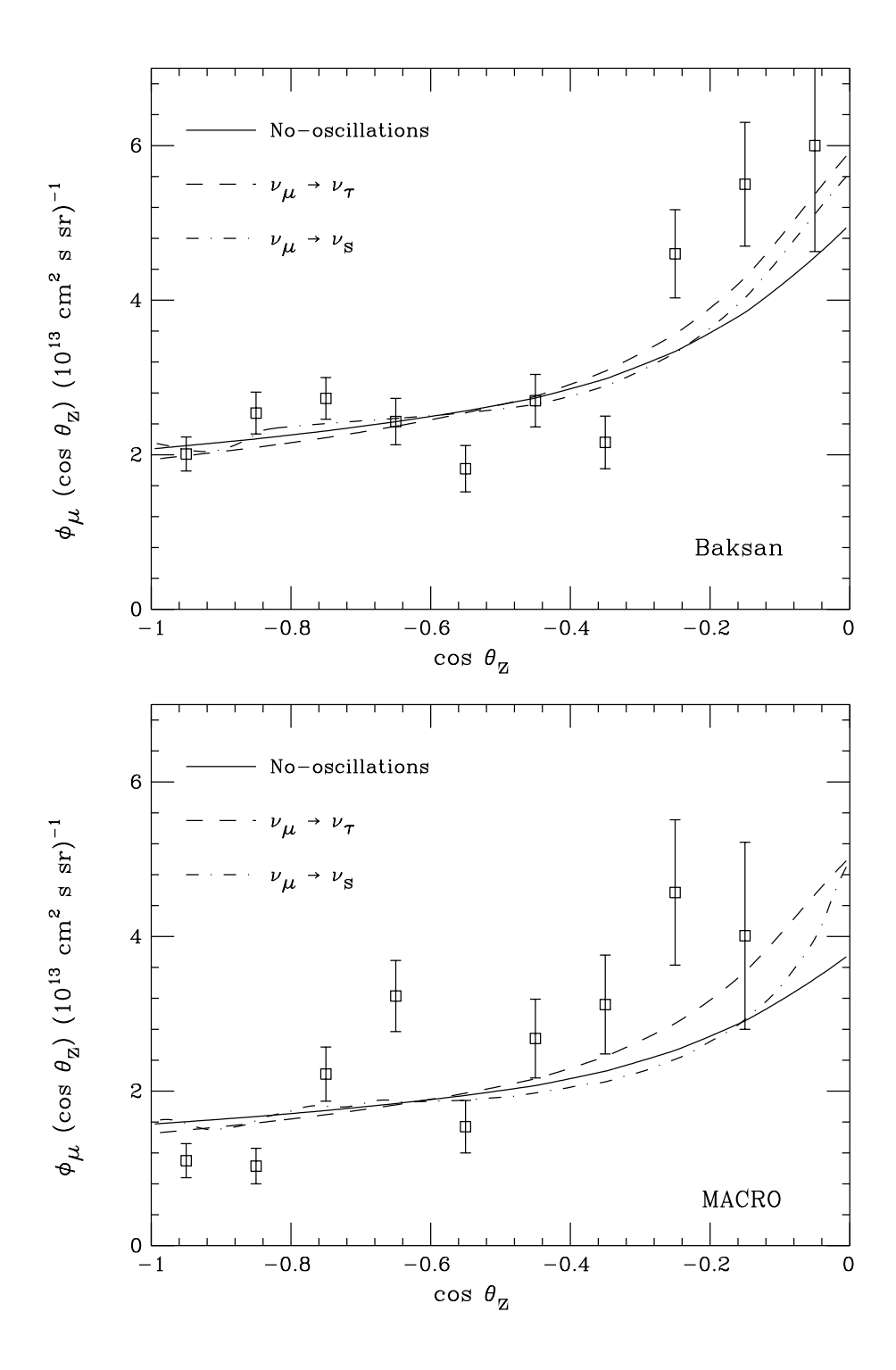


Figure 16: Flux of through–going upward going muons measured in the Baksan [38] (upper panel) and MACRO [39] (lower panel) detectors, compared to the no–oscillation hypothesis and to oscillation models for ν_{μ} – ν_{τ} and ν_{μ} – ν_{s} with best fit parameters (see text).